Electron thermal effects in standing shear Alfvén waves

P. A. Damiano[1,2] and A. N. Wright[1]

[1]   Recent hybrid MHD-kinetic electron simulations of Field Line Resonances have illustrated that the acceleration of electrons to carry the field aligned current can dissipate a significant amount of wave energy over only half an Alfvén cycle. This was done in the limit of colder electron temperatures, and in the present study we extend this to consider temperatures of up to several hundred eV. It is found that mirror force effects enhance both the parallel electric field needed to support the given current as well as the dissipation associated with the acceleration of the electrons to carry it. The current-voltage (C-V) relation appears consistent with the Knight relation for a portion of the evolution but then saturates with the decline of electrons within the loss cone.

Citation: Damiano, P. A., and A. N. Wright (2008), Electron thermal effects in standing shear Alfvén waves, *J. Geophys. Res.*, *113*, A09219, doi:10.1029/2008JA013087.

1.   Introduction

[2]   Field line resonances (FLRs) are standing Alfvén wave structures along the Earth's closed magnetic field lines that are the result of mode conversion from fast magnetoacoustic modes [e.g., *Wright and Mann*, 2006, and references therein]. They have frequencies on the order of mHz and a current system dominated by parallel electron currents closed by ion polarization currents perpendicular to the ambient magnetic field. The link between electrons accelerated along the field line by these waves and the formation of auroral arcs has been established by both satellite and ground based observations [e.g., *Xu et al.*, 1993; *Lotko et al.*, 1998; *Samson et al.*, 2003].

[3]   The dissipation of these standing modes has been traditionally associated only with ohmic dissipation within ionospheric Pedersen currents [e.g., see *Newton et al.*, 1978; *Allan and Knox*, 1979], but in recent years, it has been shown in both observations [*Chaston et al.*, 2002], two fluid theory [*Wright et al.*, 2003] and more recently hybrid MHD-kinetic simulations [*Damiano et al.*, 2007] that the acceleration of electrons to carry the field aligned current is in itself a significant sink of Alfvén wave energy that can be of the same order as ionospheric dissipation. This was not seen initially in the many single fluid studies of FLRs since in that limit the electron mass is neglected relative to the ion mass. Although this is a legitimate approximation to make, the high speed attained by electrons to carry the required field aligned current ($\sim 10^7$ m/s for $j_{\parallel} \sim \mu$A/m^2) compensates for their small mass and the resulting electron kinetic energy flux is no longer negligible when the flux tube becomes sufficiently narrow. It was found in *Damiano et al.*

[2007] that 20% of the wave energy could be dissipated in a 1/2 Alfvén period for a typical equatorial resonance width of 0.25 R_E and the dissipation increased as the width of the flux tube narrows (since the electrons must be accelerated more to carry the required current). The results of this preliminary investigation employed a cold electron population in order to understand the system in the absence of significant mirror force effects.

[4]   There has been much focus in recent years on the development of models for the self-consistent treatment of electron acceleration in Alfvén waves. These have been generally divided into efforts that have focused on Alfvén pulse phenomena [e.g., *Hui and Seyler*, 1992; *Watt et al.*, 2004, 2006; *Damiano and Wright*, 2005; *Swift*, 2007] and standing modes [*Damiano et al.*, 2003, 2005, 2007; *Rankin et al.*, 2007]. *Damiano et al.* [2007] however, was the first self-consistent treatment of a 2D FLR system in a proper 3D dipolar geometry. In this study, we extend these results by considering higher electron temperatures and explore mirror force effects on the distribution function evolution, parallel electric field generation and energy dissipation. With the higher electron temperature, the electron thermal current associated with loss cone electrons can be a significant means by which a large portion of the parallel current required by the Alfvén wave perturbation can be carried without the necessity of a parallel electric field. This source of electrons though is finite and so we will also explore the effects of an empty loss cone on the evolution of the FLR system.

[5]   The rest of the paper is broken up into four sections. Section 2 summarizes the hybrid model used here and in *Damiano et al.* [2007]. Section 3 presents the simulation results while section 4 summarizes the computed C-V relations in comparison with the Knight model and section 5 gives our conclusions.

2.   Hybrid Model

[6]   The model used is a 2-D hybrid MHD-kinetic electron model in dipolar coordinates and is fully described in

[1]Mathematical Institute, University of St. Andrews, St. Andrews, Fife, UK.
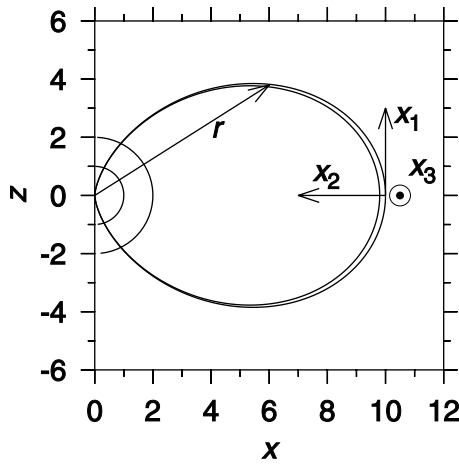[2]Now at Thayer School of Engineering, Dartmouth College, Hanover, New Hampshire, USA.

Figure 1. Simulation domain in dipolar coordinates where x_3 is positive increasing out of the page. The circle of radius 2 centered on the origin represents the "ionospheric" boundary in the present simulations. For comparison, the circle of radius 1 defines the earth's surface. θ is the angle subtended from the z axis [after *Damiano et al.*, 2007].

Damiano et al. [2007]. The geometry is illustrated in Figure 1 and explicitly includes the field aligned direction (x_1) and the direction across L shells (x_2). Our system is independent of the azimuthal coordinate so that $\partial/\partial x_3 = 0$. The model is a combination of the cold plasma MHD equations for the azimuthal perturbations of the shear velocity (u_3) and magnetic field (b_3) given respectively by

$$\mu_o \rho_o \frac{\partial u_3}{\partial t} = \frac{B_o}{h_1 h_3}\left(\frac{\partial}{\partial x_1}(h_3 b_3)\right) \quad (1)$$

$$\frac{\partial b_3}{\partial t} = \frac{-1}{h_1 h_2}\left(\frac{\partial}{\partial x_1}(h_2 E_2) - \frac{\partial}{\partial x_2}(h_1 E_1)\right) \quad (2)$$

and the guiding center equations for the electron dynamics

$$m_e \frac{dv_1}{dt} = -eE_1 - \mu_m \frac{1}{h_1}\frac{\partial B_o}{\partial x_1} \quad (3)$$

$$h_1 \frac{dx_1}{dt} = v_1 \quad (4)$$

where v_1 is the parallel electron velocity, $x_1 = \cos\theta/r^2$, $x_2 = \sin^2\theta/r$, $x_3 = \phi$, $h_1 = r^3/(1 + 3\cos^2\theta)^{1/2}$, $h_2 = r^2/(\sin\theta\,(1 + 3\cos^2\theta)^{1/2})$, $h_3 = r\sin\theta$ and $\mu_m = m_e v_1^2/(2B)$ is the magnetic moment. The solutions of the coupled equations (1) and (2) with $\mathbf{E} = -\mathbf{u}\times\mathbf{B}$ will be referred to as the MHD model. The inclusion of only the azimuthal MHD components here restricts the model to only the consideration of toroidal standing modes.

[7] Closure between MHD and electrons is via the parallel electric field given by

$$\frac{\partial}{\partial x_2}\left(\frac{h_3}{h_1 h_2}\left(\frac{\partial G}{\partial x_2}\right)\right) - \frac{G}{\lambda_e^2} = \frac{\partial}{\partial x_2}\left(\frac{h_3}{h_1 h_2}\frac{\partial}{\partial x_1}(h_2 E_2)\right)$$
$$+ e\mu_o \frac{\partial}{\partial x_1}\int v_1^2 f d^3 v$$
$$+ \mu_o \frac{e}{m_e}\frac{\partial B_o}{\partial x_1}\int \mu_m f d^3 v$$
$$- 2\mu_o \frac{e}{m_e}\frac{\partial B_o}{\partial x_1}\int \frac{m_e v_1^2}{2B_o} f d^3 v \quad (5)$$

where $\lambda_e = \sqrt{m_e/\mu_o n e^2}$ is the electron inertial length and $G = h_1 E_1$. This is a variant of the Generalized Ohm's law incorporating mirror force effects (see the work of *Damiano et al.* [2007] for derivation) where the second term on the right-hand side relates to the gradient of the electron pressure while the third and fourth terms are the perpendicular and parallel electron pressures respectively. The "classical" inertial term ($\lambda_e^2 \partial j_1/\partial t$) is incorporated into the remaining terms where E_2 is obtained from the ideal MHD approximation ($E_2 = -u_3 B_o$). The terms involving the electron pressure are calculated from the electron distribution function using Particle-In-Cell (PIC) techniques.

[8] The model equations are solved using a predictor-corrector method and equation (5) provides an estimate of parallel electric field at the predictor step. In order to enforce quasi-neutrality, any residual $\nabla\cdot\vec{j}$, is corrected for using

$$\epsilon_o \frac{\partial}{\partial t}\left(\frac{1}{h_1 h_2 h_3}\frac{\partial}{\partial x_2}(h_1 h_3 E_{2c})\right) = -\nabla\cdot\vec{j}$$
$$= \frac{-1}{h_1 h_2 h_3}\left(\frac{\partial}{\partial x_1}(h_2 h_3 j_e)\right.$$
$$\left. + \frac{\partial}{\partial x_2}(h_1 h_3 j_2)\right) \quad (6)$$

where $j_e = -e\int v_1 f d^3 v$ and E_{2c} is the correction to the perpendicular electric field. Equation (6) is derived from the continuity equations for electrons and ions and Poisson's equation. The parallel electric field is then corrected for by incorporating E_{2c} in the first term on the right-hand-side of equation (5) at the corrector step.

[9] The electrons are initialized to form a uniform distribution. The three (x_1, x_2, x_3) component electron velocities are assigned independent of each other using equal temperature maxwellians as probability weighting functions. The two perpendicular velocities for each electron are combined to form the gyroaveraged velocity perpendicular to the ambient magnetic field ($v_\perp = \sqrt{v_2^2 + v_3^2}$). This is then used to calculate the magnetic moment of the electron ($\mu_m = m_e v_\perp^2/(2B)$ - using the ambient magnetic field at the particles initial position) and in conjunction with the assigned parallel velocity $v_\| = v_1$, the initial pitch angle ($\alpha = \arctan v_\perp/v_\|$). The resulting 2D maxwellian distribution has a full loss cone. In the event that we wish to initialize the simulation with an empty loss cone (so that the thermal current $j_{th} = 0$), we must restrict equatorial pitch angles below the loss cone angle for the given field line and ionospheric altitude. This is done as follows. After the pitch angles are calculated from the component velocities, the equatorial pitch angle (α_o) is determined from the square root of the ratio of the equatorial magnetic field ($B_{o_{eq}}$) to the magnetic field at the particles position ($\alpha_o = \sqrt{B_{o_{eq}}/B_{o_e}}\,\alpha$). For an $L = 10$ field line, electrons with $\alpha_o \leq 3°$ mirror at altitudes of less than $2\,R_E$ (the present ionospheric boundary). Therefore in order to restrict j_{th} if the equatorial pitch angle of a given electron is less than $3°$ we reassign the value of the parallel velocity and repeat the procedure until the pitch angle restriction is satisfied. This choice of $2\,R_E$ (as measured from the center of the Earth) for the ionospheric boundary
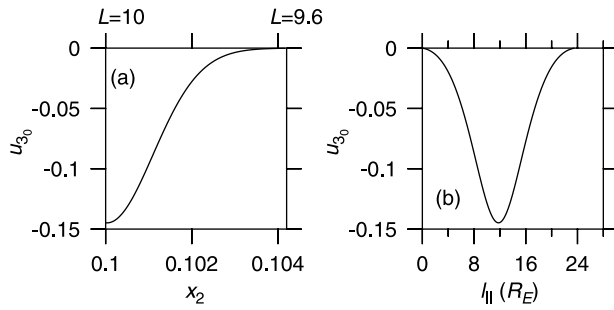
Figure 2. (a) Azimuthal velocity perturbation as a function of x_2 at the equator ($x_1 = 0$). (b) Same but as a function of length along the field line (along $x_2 = 0.1$, i.e., $L = 10$) where the length is measured from the southern ionospheric boundary [after *Damiano et al.*, 2007].

corresponds approximately with an average location for the B/n peak above which most of the electron acceleration will occur [e.g., *Wright et al.*, 2002] since as density increases into the ionosphere, less electron drift will be needed to carry the current.

[10] For the present work we do not consider the full mode conversion problem, but initialize the simulations using the same perturbation (see Figure 2) of the azimuthal velocity as used by *Damiano et al.* [2007] given by

$$u_3(x_2, x_1, t_o) = Aw(x_1)\exp\left(-\frac{(1/x_2 - 1/x_{2r})^2}{2\sigma_\perp^2}\right) \quad (7)$$

where A is the amplitude of the perturbation (set to 100 km/s), $w(x_1)$ is the approximate fundamental eigenmode solution along an $L = 10$ magnetic field line (normalized to unity at the equator) adapted from equation (32) in the work of *Wright et al.* [2002] and based on the model of *Taylor and Walker* [1984]; x_{2r} is the x_2 value at the $L = 10$ field line, and $\sigma_\perp$ is the standard deviation of the Gaussian profile. We define the equatorial wavelength $\lambda_{eq_\perp}$ of the perturbation as twice the full width at half maximum of the Gaussian profile and it is related to the standard deviation by the expression $\sigma_\perp = \lambda_{eq_\perp}/(4\sqrt{2\ln 2})$. For all runs we set $\lambda_{eq_\perp} = 0.5\ R_E$. This corresponds to the widest case considered by *Damiano et al.* [2007]. The half Gaussian profile in the perpendicular direction results in only upward field aligned currents as this is the portion of the Alfvén wave associated with downward electron acceleration. An initialization of this form, although neglecting the self-consistent evolution of the distribution function with the formative wave fields, allows us to study the simpler problem of the interaction of an equilibrium maxwellian to a shear Alfvén wave perturbation in the upward current phase of an FLR.

[11] Perfectly reflecting boundary conditions are assumed at the ionospheres ($u_3 = j_2 = \partial(h_1 j_1)/\partial x_1 = \partial(h_3 b_3)/\partial x_1 = 0$). At the perpendicular boundaries (along the lines of constant x_2) a node in current is assumed which implies nodes in E_1 and anti-nodes in b_3, j_2 and u_3 (respectively $\partial(h_3 b_3)/\partial x_2 = \partial(h_1 h_3 j_2)/\partial x_2 = \partial/\partial x_2(h_1 h_3 u_3/B_o) = 0$). The boundary condition on the electrons is handled in terms of a critical current, j_c at the ionospheric boundaries which is a function

of the noise in the parallel current averaged from 20 grid points on the opposite perpendicular boundary to x_{2r} (and hence well away from the current maximum). If the absolute value of the MHD current (in a given grid cell at the boundary) is less than the absolute value of the critical current then electrons are reflected back into the simulation domain. This approximates the upwelling of electrons of ionospheric origin (or backscattered electrons) that would naturally occur and serves to balance the thermal current associated with the loss cone electrons. Therefore there are no field aligned currents at $t = 0$ consistent with the lack of an initial magnetic field perturbation. For $|j_{MHD}| > |j_c|$, electrons that reach the boundary are allowed to precipitate and those already in the loss cone are free to support the carrying of the required MHD current without the necessity of being accelerated by the parallel electric field (as previously discussed). As the electron motion is only parallel to the magnetic field, there are no boundary conditions on them at the perpendicular edges of the grid with the exception that all the electron velocities are multiplied by a hyper-Gaussian function that goes to zero very steeply close to x_{2r} but is unity everywhere else. This is sufficiently removed from the current maximum, along which most of the analysis will be done, not to be a source of error, yet adds stability to the code. For a more complete discussion on the boundary conditions, please refer to *Damiano et al.* [2007].

[12] In the simulations to follow, all length scales are normalized by an Earth radius ($L_n = R_E$), densities by $\rho_n = 0.1\ m_p\ \text{cm}^{-3}$, magnetic fields by $B_N = 10\ nT$, velocities by $v_N = \sqrt{B_N^2/(\mu_o \rho_n)}$ and time as $t_N = L_N/v_N$. This yields normalizations for the current density and electric field as $j_N = B_N/(\mu_o L_x)$ and $E_n = v_N B_N$ respectively. Unless otherwise specified all displayed quantities are in normalized units. In all cases, 256 and 128 grid points were used in the parallel and perpendicular directions respectively, the number of simulation particles was 128 million and the time step was 0.002 seconds. A constant plasma number density of $n = 10^6\ \text{m}^{-3}$ was chosen everywhere along the field line which results in a period of oscillation of about 270 seconds for the $L = 10$ field line considered. In the present simulations however, we let the system evolve for only a 1/4 period ($t \approx 70$ s) to reach the level of maximum field aligned current.

3. Simulations

[13] In this section we compare three simulations with electron temperatures of 5, 50 and 200 eV. All other parameters are the same. Figure 3 displays the parallel current at the northern ionospheric boundary as a function of x_2 at $t = 20$, 50 and 70 seconds (1/4 period) for all three cases along with the solution of the cold plasma MHD model. There is an initial close correspondence between all three temperature results and the MHD, but differences become evident as the system evolves particularly for $T_e = 200$ eV. In this latter case, there is also a clear widening of the current profile across the width of the simulation domain. This widening is consistent with results observed in *Damiano et al.* [2007], with the exception that the widening was mostly manifest in the case of narrower current profiles. More comment will be made on this later.
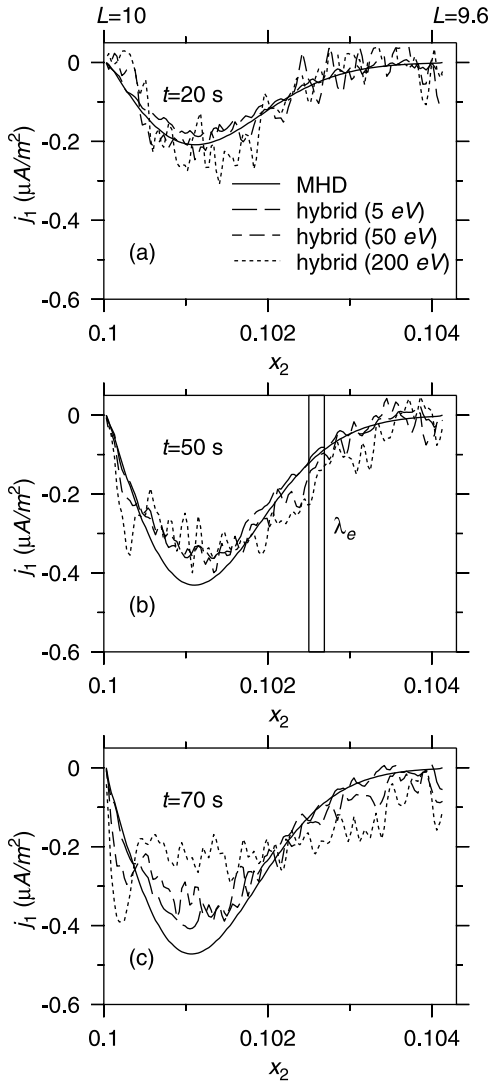
Figure 3. Parallel current density at the northern ionospheric boundary at (a) $t = 20$ s, (b) $t = 50$ s, and (c) $t = 70$ s (values averaged with adjacent grid cells for smoothness). The double lines in Figure 3b indicate the electron inertial length λ_e.

[14] A scatter plot of the electrons at the northern ionospheric boundary at the location where the MHD solution has the maximum current ($0.1008 \leq x_2 \leq 0.1012$) is plotted in Figure 4f for $T_e = 50$ eV at $t = 50$ seconds. Figures 4a–4e are plots of the same electrons at previous times (and hence further up the field line). It is important to note that the individual electrons have different positions along the field line depending on their speed and energy and are only truly "local" to each other in Figure 4f. In Figure 4a, the semi-circular path exhibited by a portion of the electrons are those which are mirrored at the southern ionospheric boundary (after being partially accelerated to carry the field aligned current) and are travelling back up the field line forming the narrow peak ahead of the bulk in Figure 4b. These are in-turn the first to be mirrored again as the northern ionospheric boundary is approached and evolve to form the tail of the ring distribution illustrated in Figure 4f). The total kinetic energy ($1/2 \, m_e v^2$) is relatively

constant from Figures 4a to 4d, increases by about 10% in between Figures 4d and 4e and by about 25% between Figures 4e and 4f. Therefore a majority of the acceleration is happening in the final couple of seconds before the electrons reach the ionospheric boundary.

[15] Figures 4a–4f illustrate the acceleration of the electrons to carry the current, but not where the acceleration is happening along the field line. In Figure 5, we plot the current density along $x_2 = 0.101$ as a function of distance along the field line (for the same time and temperature as Figure 4) as well as the distribution function at the ionospheric boundary (Figure 5c) and at a distance of 10 R_E from the equator (Figure 5b). The jump in current evident in the last couple of earth radii before the ionosphere is consistent with the increase in the parallel drift of the electrons in the distribution function illustrating that a majority of the acceleration is happening in this region. The distribution function plotted in Figure 5c is made using
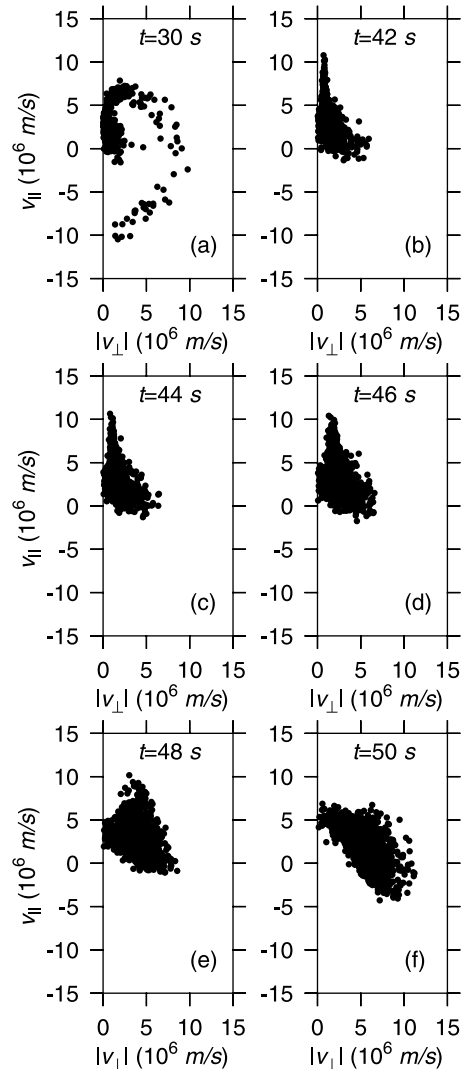

Figure 4. Time evolution of the distribution of electrons carrying current at the northern ionospheric boundary at $t = 50$ s for $T_e = 50$ eV. Scatter plot for $t = 50$ s compiled from electrons with radial positions $0.1008 \leq x_2 \leq 0.1012$ in the last line of grid cells before the ionospheric boundary.
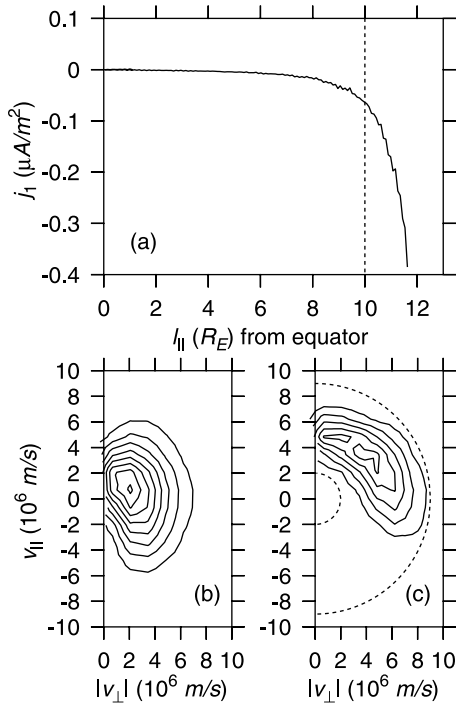
Figure 5. (a) Parallel current density along $x_2 = 0.101$ as a function of distance along the field line, $l_{\parallel}$ (as measured from the equator) at $t = 50$ s for $T_e = 50$ eV. (b) Distribution function at $l_{\parallel} = 10\ R_E$. (c) Distribution function at the ionospheric boundary. Dotted lines in Figure 5c are lines of constant total velocity v, for $v = 2 \times 10^6$ and $v = 9 \times 10^6$ m/s.

the same electrons as the scatter plot in Figure 4f and has a radius of roughly constant total velocity, v.

[16] Figure 6 illustrates the distribution function at the ionospheric boundary at $t = 50$ seconds for all three electron temperatures considered. The field aligned currents noted in Figure 3 are similar at these times and so the effect of the temperatures on the electron drift can be contrasted. The parallel drift increases with temperature as does the radius of the arc in velocity space. This can be interpreted as follows. As temperature increases a larger fraction of the accelerated electrons will experience a mirror force sufficiently strong to overcome the force associated with the downward parallel electric field and so end up travelling back up the field line in the wrong direction to carry the required current. Therefore the remaining downwelling population must be accelerated to higher parallel velocity to compensate (in analogy to $j_1 = -nev_d$ where v_d is the drift velocity of the electrons). As a comparison, in the 5 eV case, electrons are being accelerated to an energy on the order of 10 eV, while in the 200 eV case, the energy is on the order of 100 eV.

[17] Since the time scale of electron acceleration (a few seconds) is much less than the wave period, we can consider the electric field to be quasi-static and introduce a potential ϕ. Energy conservation may be expressed as

$$e\Delta\phi = \frac{1}{2}m_e\left(v_{\parallel}^2 + v_{\perp}^2\right). \tag{8}$$

It is clear that the increased radius of the ring distribution implies that the electrons have fallen through a larger potential drop (and thus experienced a larger electric field on average) in order to be sufficiently accelerated to carry the required current. This point will be returned to shortly. Close to the ionospheric boundary, as many of the electrons begin to mirror the parallel velocity gained by the acceleration is transferred to perpendicular velocity (accounting for the formation of the partial ring in velocity space).

[18] Another interesting point is that in the $T_e = 200$ eV case there is a definite thinning of the number of electrons available at small pitch angles. This is further evident in Figure 7 where the distribution function of the ionospheric boundary is plotted again at $t = 50$ s and later times. By $t = 70$ s, there are essentially no electrons available at small pitch angles to carry the current. This corresponds approximately with the widening of the current profile for $T_e = 200$ eV evident in Figure 3 and the integrated current across the simulation domain is consistent with that determined for the $T_e = 5$ and $T_e = 50$ eV profiles in the same figure to within 10%. Therefore it appears that although electrons are getting accelerated along adjacent field lines for $T_e = 200$ eV, a similar total current is being carried in all three cases.

[19] It is not clear by which mechanism the flux tube broadens, but it is suggestive that some of the fluctuations in Figure 3 are larger than $2\Delta x_2$ and on the order of the electron inertial length or a multiple thereof. Since inertial Alfvén waves can propagate perpendicular to the magnetic field for $\lambda_{\perp} \sim \lambda_e$, it is possible that electron inertial effects
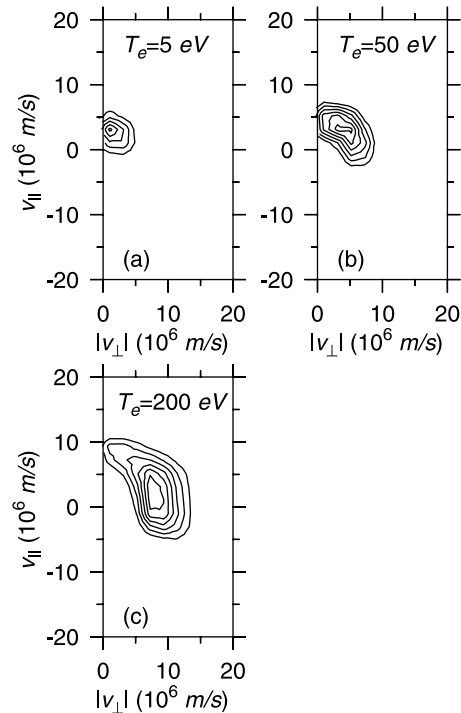

Figure 6. Distribution function at the northern ionospheric boundary for $t = 50$ s and (a) $T_e = 5$ eV, (b) $T_e = 50$ eV, and (c) $T_e = 200$ eV. Distribution functions are compiled from electrons with radial positions $0.1008 \le x_2 \le 0.1012$ in the last line of grid cells before the ionospheric boundary. Contour intervals are constant in each figure but differ between figures.
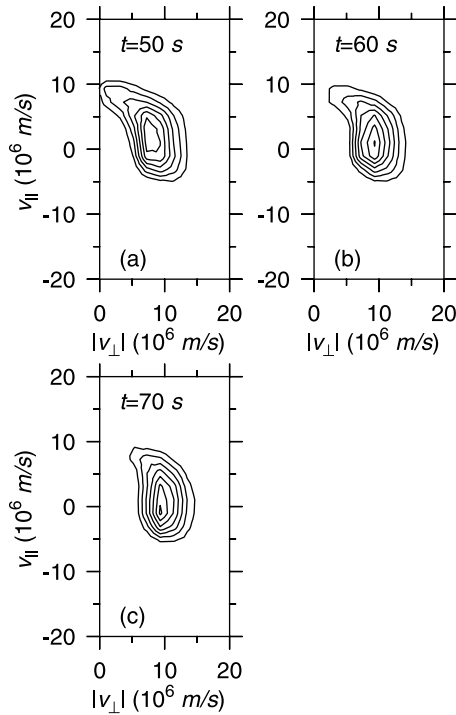
Figure 7. Distribution function at the northern ionospheric boundary for $T_e = 200$ eV at the indicated times. Distribution functions are compiled from electrons with radial positions $0.1008 \leq x_2 \leq 0.1012$ in the last line of grid cells before the ionospheric boundary. Contour levels are constant in all figures.

because of the large bin size needed to bring out the details further down the field line, the gradient of the contours steepens within the last couple of earth radii before the ionospheric boundary indicating where most of the electron acceleration is taking place (consistent with Figure 5). Examination of these profiles at several times indicate that the basic characteristics remain the same for the length of the simulation.

[21] The parallel current density along the field line at $x_2 = 0.101$ is plotted in Figure 9a for all three temperatures at $t = 50$ s. For smoothness, each profile is an
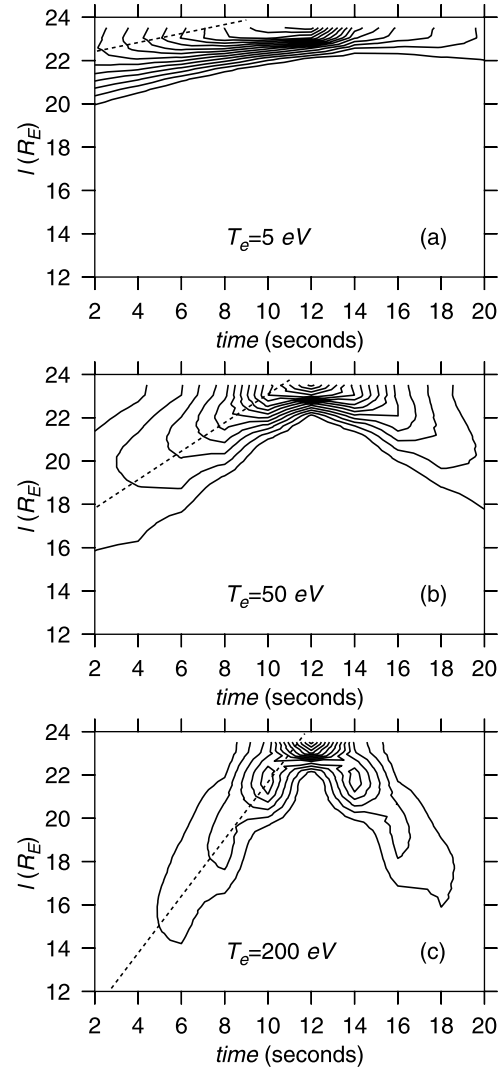
play some role in the broadening. This point is beyond the scope of the present work though and will be addressed more fully in the future.

[20] Figure 8 displays the time history of the electron population carrying the ionospheric current at $t = 12$ for all three electron temperatures. This is displayed in terms of electron number densities in l (distance along the field line) as measured from the southern ionospheric boundary. They were determined by following the electrons with radial positions between $0.1008 \leq x_2 \leq 0.1012$ at the ionospheric boundary at $t = 12$ seconds both backward and forward (unless precipitated) in time for each of the temperatures. A histogram was then created of electron number per length interval along the field line at each individual time (2 seconds intervals were used). The individual histograms were then stacked to form the series in time and the 2-D data displayed with the use of contours. The data for the individual bins in each histogram was plotted in the middle of the interval for the contours and the contour levels are the same in each figure. As temperature increases, the source of electrons extends further down the field line with a fairly constant slope. Superimposed on the contours (with a dotted line) is a slope defined by the thermal velocity of the distribution function ($v_{th} = \sqrt{2T_e/m_e}$) illustrating that there is an excellent agreement between the two. This implies that the current carrying electrons are travelling freely down the field line with an average velocity defined by the thermal velocity of the distribution function. Although not exceptionally clear

Figure 8. Distribution of electrons along the field line as a function of time for the electron population carrying the current at the ionospheric boundary at $t = 12$ s for all three temperatures. Plots were created by taking the electrons which formed the distribution functions between $0.1008 \leq x_2 \leq 0.1012$ (parallel current density maximum) at the northern ionospheric boundary for $t = 12$ s and then following the individual particles backward and forward in time. The positions of all the electrons at each time were then binned as a function of length along the field line. Contour increments are equal and increasing toward the ionosphere and $t = 12$ s.
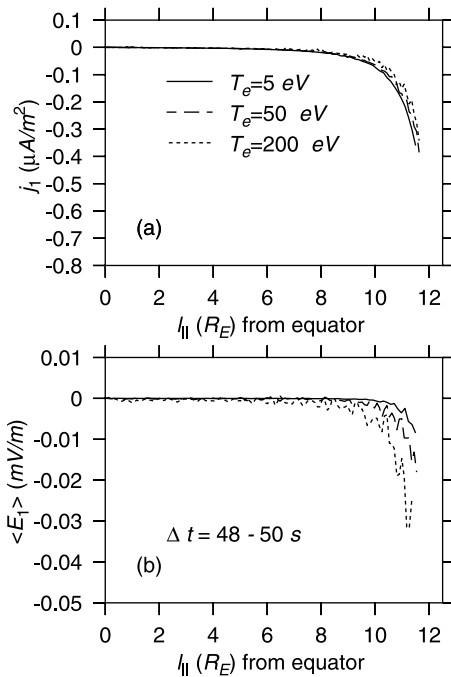
Figure 9. (a) Parallel current density and (b) parallel electric field along $x_2 = 0.101$ at $t = 50$ s. The parallel electric field is the average over the indicated time interval.

average of the five grid lines of constant x_2 adjacent to either side of the grid line of interest. All three profiles are still approximately equal at this time increasing proportional to B_o toward the ionospheric boundary, as the flux tube narrows. The fact that the three current densities are similar allows for a comparison of the parallel electric field profiles needed to sustain the current for each of the different temperatures. These profiles are not the instantaneous electric field which is difficult to resolve because of the statistical nature of the model and the relatively small values of the parallel electric field. However, the fields can be resolved by time averaging over a specified interval and then spatially averaging over adjacent grid cells. For the results presented in Figure 9b, the parallel electric field is time averaged over the interval from 48–50 seconds to correspond closely to the time of the displayed current density results. For consistency, these parallel electric field profiles are also spatially averaged with adjacent field lines as discussed for the current density above. Evident is a clear enhancement of the profile along the field line as the initial electron temperature is increased.

[22] This enhancement must be examined in both the context of increased mirror force and increased thermal current. The latter is the current density due to the downgoing electron population (equal to the loss cone population at the ionospheric boundary) and is given by

$$j_{th} = -e \int_0^\infty v_\| f dv_\| \int_0^\infty 2\pi v_\perp dv_\perp = -en_o \sqrt{\frac{kT}{2\pi m_e}} \quad (9)$$

[e.g., see *Cran-McGreehin and Wright*, 2005; *Shiokawa et al.*, 2000]. For the $T_e = 50$ eV and 200 eV, j_{th} is about 0.2

and 0.4 μA/m^2 respectively. Therefore the loss cone electrons alone can support a good portion of the current evident in the present simulations without the need for a parallel electric field. However, the length of time a thermal current can be sustained in a given flux tube is inversely proportional to the temperature (unless the loss cone is being replenished by some mechanism such as the influx of ionospheric electrons or pitch angle diffusion, but this in beyond the scope of this present work). Test particle simulations of the present flux tube configuration with $T_e = 200$ eV illustrated that the thermal current was about half its initial value by about $t = 30$ seconds and completely dissipated by about 50 seconds. Correspondingly, the thermal current in the $T_e = 50$ eV case was sustained at more or less a constant level for almost a full quarter Alfvén period, starting to diminish significantly after about 60 seconds. The initial values of the currents in both cases showed good agreement with the values predicted by equation (9) (within about 10%).

[23] The present coupled model restricts the flow of the thermal current because of the reflecting boundary condition involving the critical current j_c which operates at early times. However, this does not restrict the availability of these loss cone electrons as the perturbation current grows. Once the loss cone is emptied, the parallel electric field must act on the remaining trapped population to accelerate the electrons necessary to carry the current. Since, the distribution function widens as temperature increases, the number of electrons experiencing a larger mirror force increases and an enhanced electric field is needed to sustain a given current. The results presented here are not the first to illustrate the effect of mirror force effects on the parallel electric field. This was examined in the limit of a DC current and static potential drop along the field line by *Knight* [1973], for Alfvén wave pulses by *Nakamura* [2000] and in the context of field line resonances by *Rankin et al.* [1999]. The latter considered the relation between E_1 and j_1 through a "non-local" conductivity which results from the mirror force trapping of electrons in their linearized model.

[24] The ability of the parallel electric field to replenish the loss cone was tested by initializing the electrons so that the loss cone was not populated at $t = 0$ as discussed previously. This was done for $T_e = 50$ eV. It was found that there was very little difference in the evolution of the system when contrasted with the same temperature simulation with the loss one full. There was a slightly larger decrease in wave energy which is a result of the extra work being done on the electrons to allow them to precipitate in the ionosphere. Presumably, there was a larger parallel electric field early on as well to facilitate this, but the difference is too small to be clearly discernible because of the noise. Therefore to a degree the parallel electric field is able to fill the nominal loss cone without significantly altering the evolution of the system. However, as the current continues to grow and electrons that are easy to accelerate become less accessible, the system must work harder to continually supply electrons along a given flux tube. At some point, it appears to become easier to accelerate electrons along adjacent field lines as evidenced by the broadening in Figure 3. In this present case, the mirror force associated with the higher temperature is what is restricting the electrons along the flux tube. In the work of *Damiano et*
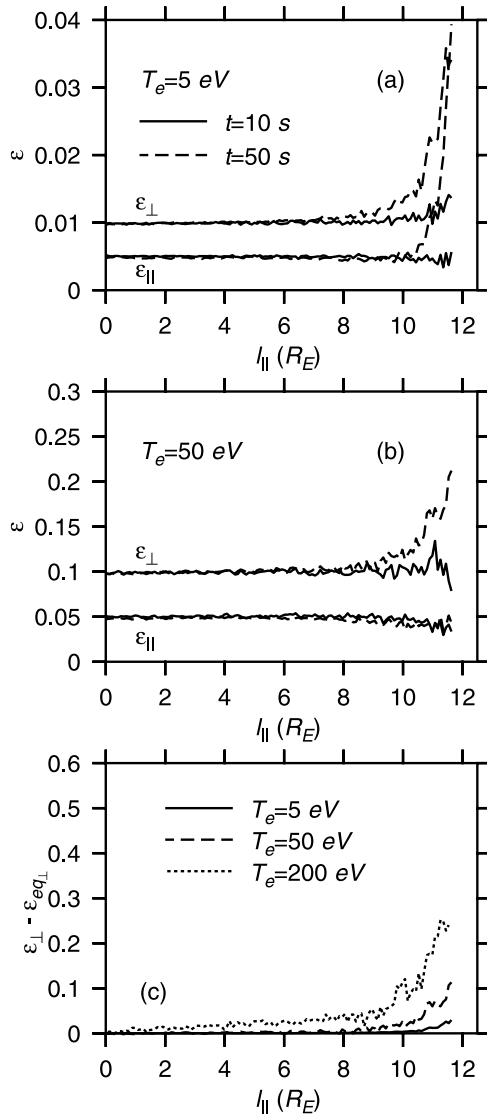
Figure 10. Electron energy density along the field line as measured from the equator broken up into parallel and perpendicular velocity components for (a) $T_e = 5$ eV and (b) $T_e = 50$ eV. Figure 10c illustrates the perpendicular electron energy density profiles for all three temperatures (at $t = 50$ s) with the approximate background energy ($\epsilon_{eq} = \epsilon_\perp$ at the equator) in each case subtracted off.

al. [2007], this broadening appeared for narrower flux tubes for which the current was higher. Therefore although there was less restriction in terms of a mirror force, more work was done on the electrons as they attempted to carry a larger current.

[25] Figures 10a and 10b display the electron energy densities along the field line at $x_2 = 0.101$ for $T_e = 5$ eV and $T_e = 50$ eV respectively. In both cases, results are shown for $t = 10$ and $t = 50$ seconds and the energy densities are broken up into parallel ($\epsilon_\parallel$) and perpendicular ($\epsilon_\perp$) values (determined respectively from the second moments of the electron distribution function for $v_\parallel$ and $v_\perp$). For $T_e = 5$ eV both profiles increase as one approaches the ionospheric boundary. This increase in energy is associated with the drift in the distribution function to carry the current in the

parallel component with a portion of this energy being transferred to $v_\perp$ via the mirror force, increasing as the ionospheric boundary is approached. The background energy which approaches a constant level toward the equator, is associated with the thermal energy of the distribution function. The background energy density in $v_\perp$ is twice that of $v_\parallel$ since $v_\perp$ is the gyroaveraged velocity of the two perpendicular components.

[26] The case is somewhat different in Figure 10b where the profile in parallel energy density decreases slightly as the ionosphere is approached. This is because the thermal background energy dominates over the energy associated with the drift of the current carrying electrons and the decrease in the profile is since the latter are being lost from the system. The perpendicular energy density increases because of the mirroring electron population which remain within the flux tube.

[27] In Figure 10c, the approximate background thermal energy associated with $v_\perp$ (defined as $\epsilon_\perp$ at the equator) is subtracted off and the perpendicular energy profiles in all three cases are displayed for $t = 50$ seconds. The increased mirror force effects associated with the rise in temperature translates any enhancement in $v_\parallel$ needed to carry the current into $v_\perp$ (and hence $\epsilon_\perp$). In the 200 eV case, the increased energy density almost all the way to the equator is illustrative of the acceleration of a significant number of electrons all along the field line.

[28] Figure 11a displays the component energies for the $T_e = 50$ eV case. Ion kinetic energy in u_3 is being transferred into magnetic field energy (b_3) and electron kinetic energy. The effect of electron temperature on this energy balance is evident in Figure 11b where the energy in b_3 for the different temperatures is plotted. Energy dissipation from the wave increases with temperature as less ion kinetic energy is being transferred into the magnetic field at the expense of more being transferred into the electrons. This is consistent with the picture that has emerged in Figure 3 at a quarter period where the maximum parallel current density has decreased with increasing electron temperature. Moreover, at higher temperatures, the precipitating population has a larger $v_\perp$ (see Figure 6) and have had more work done on them, resulting in less ion kinetic energy being transferred into the magnetic field.

[29] In reality, FLRs are driven for a portion of their evolution at least and so energy would be entering the Alfvén wave over a period of time. Therefore the dissipation would be balanced to an extent by energy entering the system. If this energy is greater than the dissipation due to either electron acceleration or ohmic dissipation it would be possible for larger field aligned currents to result than those noted here. In order to attain larger currents in the current approximation, we are limited to initializing the system with a larger amplitude perturbation. A test was performed by repeating the $T_e = 200$ eV case but with a perturbation amplitude of 200 km/s. The result was that the hybrid model attained a slightly higher maximum current of about 0.5 μA/m^2 and then started to broaden in profile a little earlier than the $A = 100$ km/s case (at about $t = 50$ s). The emptying of the distribution for small pitch angles was also evident at about the same time. Therefore the evolution follows the same basic profile as already noted. Correspondingly, a run done
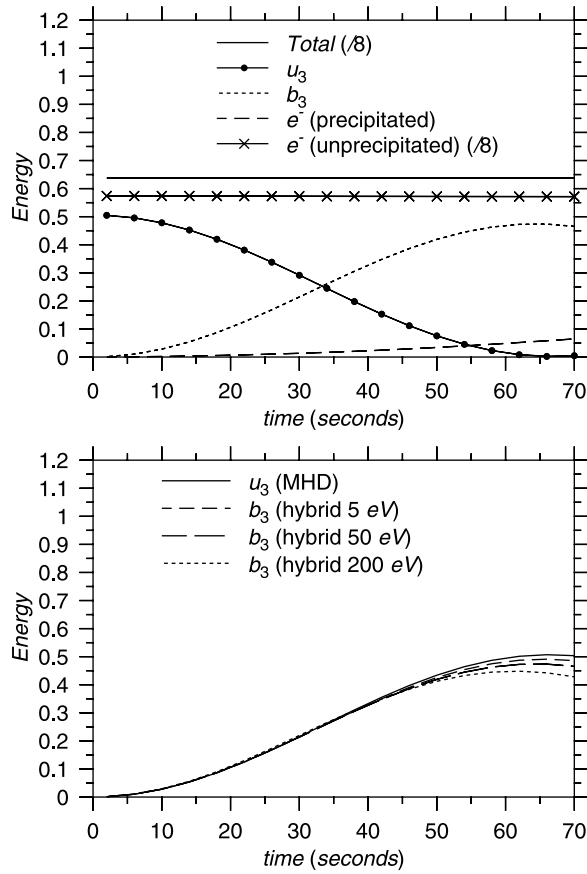
Figure 11. (top) Component energies for $T_e = 50$ eV case. The total energy and energy in the unprecipitated electron population are divided by 8 to fit on the plot. (bottom) Energy in b_3 at indicated electron temperatures.

with $A = 100$ km/s but with an initial temperature of 400 eV also showed an empty loss cone and broadening earlier on when contrasted with the 200 eV simulation presented here.

4. Current-Voltage Relation

[30] The widely used Knight relation [*Knight*, 1973] expresses the current-voltage (C-V) relation along an auroral field line and since it is linear for a good range of auroral parameters is often approximated by

$$j_1 \approx -K\Delta\phi \qquad (10)$$

where j_1 is the field aligned current at the end of the potential drop $\Delta\phi$ (usually measured from the equatorial region) and $K = n_e e^2/\sqrt{2\pi m_e kT}$. It is derived under the assumptions of adiabatic electrons, an electrostatic potential ϕ, a Maxwellian distribution function and a full loss cone. Although FLRs are not static, the transit time of the electrons along the field line is very short compared to the Alfvén period and so it is appropriate to expect the Knight relation to have some utility in the limit of our low frequency oscillations. In order to confirm this, the potential

drop along the field line was determined by the integration of the parallel electric field profiles as

$$\Delta\phi = -\int_0^{l_{ionosphere}} dl E_1 \qquad (11)$$

where l is the distance along the field line measured from the equator. As in Figure 9b, two second averaged electric field profiles along $x_2 = 0.101$ were used from $t = 2$ to $t = 70$ s and the calculated potential drop was plotted against the current at the northern ionospheric boundary (at the same value of x_2) for the time marking the end of the averaging interval. This was done for all three electron temperatures and the results are plotted in Figure 12 where
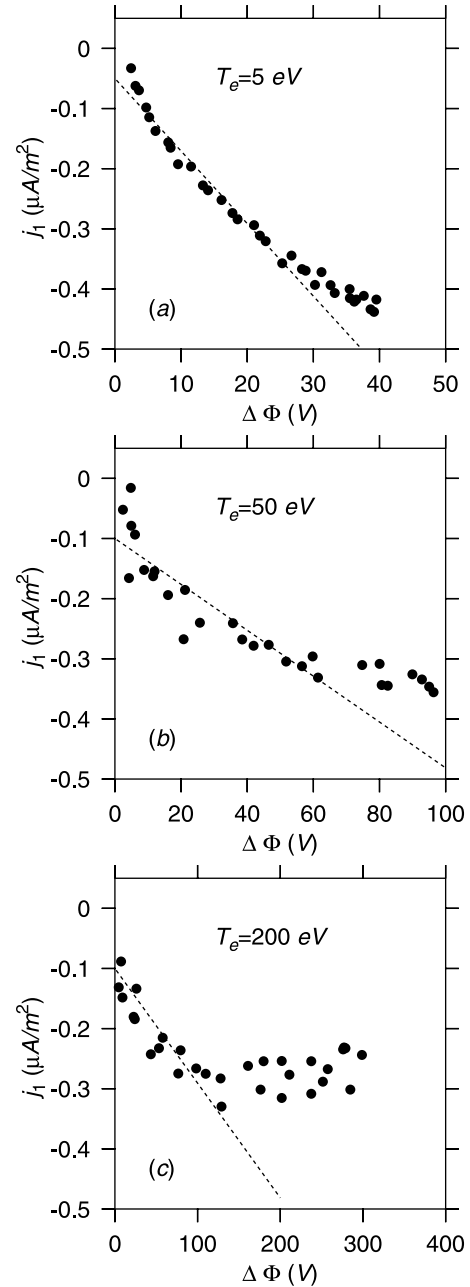

Figure 12. Current-voltage (C-V) relation along the $x_2 = 0.101$ field line for (a) $T_e = 5$ eV, (b) $T_e = 50$ eV, and (c) $T_e = 200$ eV.
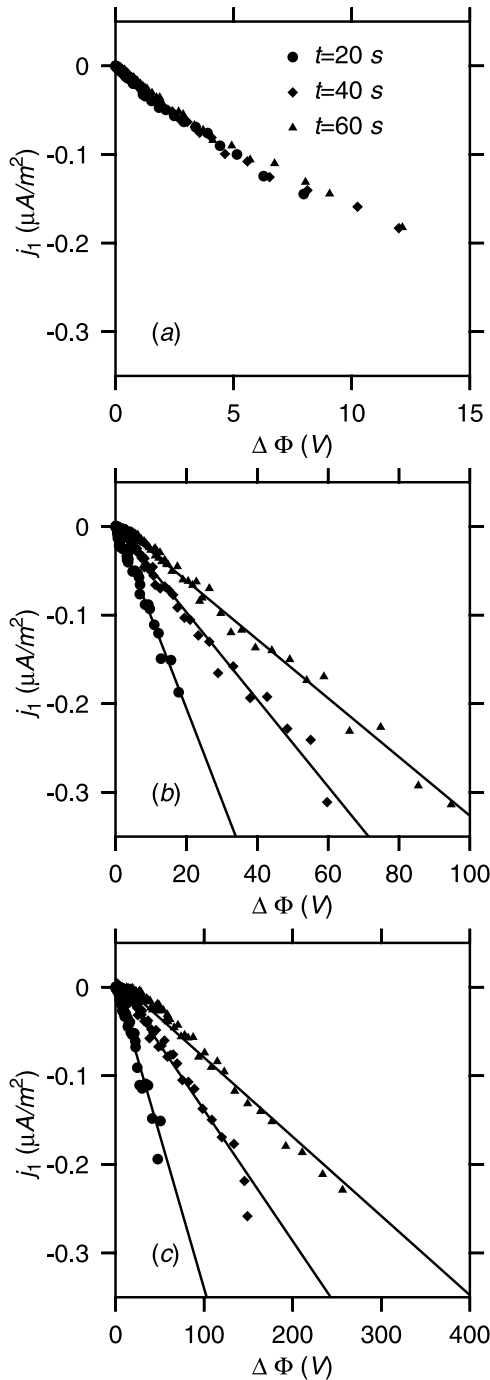
Figure 13. Current density profile along $x_2 = 0.101$ plotted against the profile of potential along the same field line at the indicated times for (a) $T_e = 5$ eV, (b) $T_e = 50$ eV, and (c) $T_e = 200$ eV. Solid lines in Figures 13b and 13c are linear regression fits through the data at the indicated times.

we have chosen the intercepts of the lines so that they clearly pass through the simulation data. Superimposed on the plots is the solution of equation (10) (dashed line) for the indicated temperatures. In all cases, there seems to a strong correspondence between the slope predicted by equation (10) and the slope followed by the simulation data. In the cases of $T_e = 50$ and $T_e = 200$ eV, especially in the

latter, there is a clear shift in the slope of the simulation data to one of constant current. This corresponds to the levels where the current reaches saturation. The increasing potential for constant current is indicative of the efforts of the model to accelerate larger pitch angle electrons to carry the current.

[31] Although the Knight relation determines the total potential drop along the current carrying flux tube, it does not prescribe how ϕ varies along the length of the tube. This is, however, something that our simulation will readily provide. In Figure 13 the current density along the $x_2 = 0.101$ field line versus the potential profile along the same field line at the specified times are shown. The points of low j_1 values correspond to points on the field line near the equator, whilst the larger currents correspond to the iono-spheric end. The potential profiles were determined using the same two second time averaged parallel electric field profiles as previously. In the case of the increased temper-atures, there is significant change in the slope of the profile with time as the potential must increase to allow electrons from outside the nominal loss cone to carry the required current. It is interesting that despite these changes the profile is remarkably linear for the range of times consid-ered. This implies that since current is directly proportional to the magnetic field when density is constant, the profile of $\Delta\phi$ must follow that of the ambient magnetic field strength as well.

5. Conclusions

[32] A 2D hybrid MHD-kinetic electron model in dipolar coordinates has been used to study the electron response to a fundamental mode Alfvén wave perturbation centered on an $L = 10$ magnetic field line for three different electron temperatures (5, 50 and 200 eV). The perpendicular profile of the perturbation was chosen so that only upward field aligned currents were considered (corresponding to down-welling electrons) and the field aligned fundamental eigen-mode for the velocity was based on the model of *Taylor and Walker* [1984] and is consistent with the perturbation used in *Damiano et al.* [2007].

[33] It was found that a ring distribution in velocity space formed close to the ionospheric boundary as some electrons accelerated to carry the current were mirrored by the converging magnetic field. This distribution formed a radius of constant total velocity which increased as the temperature did for a given current density. The increase was due to the fact that as more electrons are mirrored and begin travelling up the field line, the remaining downward propagating electrons must travel faster to carry the current. This was accompanied by a increased parallel electric field in order to facilitate the increased electron acceleration. Also, although higher temperatures implies a higher thermal current, this source of "free" electrons is diminished quickly in the model and the system must work to facilitate the accelera-tion. After a certain point, the ability of the model to accelerate the electrons along the original flux tube becomes impeded because of the lack of accessible current carriers and so the current profile broadens as electrons are accel-erated along adjacent field lines.

[34] In addition, the current-voltage (C-V) relation gen-erated from the model was compared with that predicted by

the Knight relation. There appeared to be general agreement between the two for a significant portion of the current range, but then the slope of the C-V profile in the simulated case tended to zero as the current saturated.

[35] Finally, it is worth noting that this work was designed to illustrate mirror force effects clearly for somewhat idealized conditions. Real magnetospheric temperatures are on the order of a keV and the B/n peak can occur lower than the 2 R_E noted here. Therefore both the dissipation and electric field generation as presented are lower limits to what could occur. The dissipation would also increase with time as the resonance narrows because of phase mixing over several Alfvén cycles (as discussed by *Damiano et al.* [2007]) and the mirror force (and parallel electric field itself as noted by *Rankin et al.* [2007]) can act to trap electrons over several cycles.

References

Allan, W., and F. B. Knox (1979), A dipole field model for axisymmetric Alfvén waves with finite ionospheric conductivities, *Planet. Space Sci.*, 27, 79–85.

Chaston, C. C., J. W. Bonnell, L. M. Peticolas, C. W. Carlson, J. P. McFadden, and R. E. Ergun (2002), Driven Alfvén waves and electron acceleration: A FAST case study, *Geophys. Res. Lett.*, 29(11), 1535, doi:10.1029/2001GL013842.

Cran-McGreehin, A. P., and A. N. Wright (2005), Current-voltage relationship in downward field-aligned current region, *J. Geophys. Res.*, 110, A10S10, doi:10.1029/2004JA010870.

Damiano, P. A., and A. N. Wright (2005), Two-dimensional hybrid MHD-kinetic simulations of an Alfvén wave pulse, *J. Geophys. Res.*, 110, A01201, doi:10.1029/2004JA010603.

Damiano, P. A., R. D. Sydora, and J. C. Samson (2003), Hybrid magneto-hydrodynamic-kinetic model of standing shear Alfvén waves, *J. Plasma Phys.*, 69, 277–304.

Damiano, P. A., A. N. Wright, R. D. Sydora, and J. C. Samson (2005), Hybrid magentohydrodynamic-kinetic electron closure methods and shear Alfvén waves in nonuniform plasmas, *Phys. Plasmas*, 12, 042105.

Damiano, P., A. A. N. Wright, R. D. Sydora, and J. C. Samson (2007), Energy dissipation via electron energization in standing shear Alfvén waves, *Phys. Plasmas*, 14, 062904.

Hui, C. H., and C. E. Seyler (1992), Electron acceleration by Alfvén waves in the magnetosphere, *J. Geophys. Res.*, 97, 3953–3963.

Knight, S. (1973), Parallel electric fields, *Planet. Space Sci.*, 21, 741–750.

Lotko, W., A. V. Streltsov, and C. W. Carlson (1998), Discrete auroral arc, electrostatic shock and suprathermal electrons powered by dispersive, anomalously resistive field line resonance, *Geophys. Res. Lett.*, 25, 4449–4452.

Nakamura, T. (2000), Parallel electric field of a mirror kinetic Alfvén wave, *J. Geophys. Res.*, 105, 10,729–10,737.

Newton, R. S., D. J. Southwood, and W. J. Hughes (1978), Damping of geomagnetic pulsations by the ionosphere, *Planet. Space Sci.*, 26, 201–209.

Rankin, R., J. C. Samson, and V. T. Tikhonchuk (1999), Parallel electric fields in dispersive shear Alfvén waves in the dipolar magnetosphere, *Geophys. Res. Lett.*, 26, 3601–3604.

Rankin, R., C. E. J. Watt, and J. C. Samson (2007), Self-consistent wave-particle interactions in dispersive scale long-period field line resonances, *Geophys. Res. Lett.*, 34, L23103, doi:10.1029/2007GL031317.

Samson, J. C., R. Rankin, and V. T. Tikhonchuk (2003), Optical signatures of auroral arcs produced by field line resonances: Comparison with satellite observations and modeling, *Ann. Geophys.*, 21, 933–945.

Shiokawa, K., W. Baumjohann, G. Haerendel, and H. Fukunishi (2000), High- and low-altitude observations of adiabatic parameters associated with auroral electron acceleration, *J. Geophys. Res.*, 105, 2541–2550.

Swift, D. W. (2007), A two-dimensional particle code simulation of inertial Alfvén waves and auroral electron acceleration, *J. Geophys. Res.*, 112, A01204, doi:10.1029/2006JA011998.

Taylor, J. P. H., and A. D. M. Walker (1984), Accurate approximate formulae for toroidal standing hydromagnetic oscillations in a dipolar geomagnetic field, *Planet. Space Sci.*, 32, 1119–1124.

Watt, C. E. J., R. Rankin, and R. Marchand (2004), Kinetic simulations of electron response to shear Alfvén waves in magnetospheric plasmas, *Phys. Plasmas*, 11, 1277–1284.

Watt, C. E. J., R. Rankin, I. J. Rae, and D. M. Wright (2006), Inertial Alfvén waves and acceleration of electrons in nonuniform magnetic fields, *Geophys. Res. Lett.*, 33, L02106, doi:10.1029/2005GL024779.

Wright, A. N., and I. R. Mann (2006), Global MHD eigenmodes of the outer magnetosphere, in *Magnetospheric ULF Waves: Synthesis and New Directions, Geophys. Monogr. Res.*, vol. 169, edited by K. Takahashi et al., pp. 51–72, AGU, Washington, D. C.

Wright, A. N., W. Allan, M. S. Ruderman, and R. C. Elphic (2002), The dynamics of current carriers in standing Alfvén waves: Parallel electric fields in the auroral acceleration region, *J. Geophys. Res.*, 107(A7), 1120, doi:10.1029/2001JA900168.

Wright, A. N., W. Allan, and P. A. Damiano (2003), Alfvén wave dissipation via electron energization, *Geophys. Res. Lett.*, 30(16), 1847, doi:10.1029/2003GL017605.

Xu, B. L., J. C. Samson, W. W. Liu, F. Creutzberg, and T. J. Hughes (1993), Observations of optical aurora modulated by resonant Alfvén waves, *J. Geophys. Res.*, 98, 11,531–11,541.

————————————

P. A. Damiano, Thayer School of Engineering, Dartmouth College, 8000 Cummings Hall, Hanover, NH 03755-8000, USA. (peter.damiano@dartmouth.edu)

A. N. Wright, Mathematical Institute, University of St. Andrews, North Haugh, St. Andrews, Fife KY16 9SS, UK.